Decoherence and Relaxation in Driven Circuit QED Systems

Stephan André*, Valentina Brosco*, Arkady Fedorov†, Gerd Schön* and Alexander Shnirman**

*Institut für Theoretische Festkörperphysik and DFG-Center for Functional Nanostructures (CFN), Universität Karlsruhe, D-76128 Karlsruhe, Germany
†Kavli Institute of Nanoscience, Delft University of Technology, 2600 GA Delft, The Netherlands
**Institut für Theorie der Kondensierten Materie and DFG-Center for Functional Nanostructures (CFN), Universität Karlsruhe, D-76128 Karlsruhe, Germany

Abstract. Recent experiments on quantum state engineering with superconducting circuits realized concepts originally introduced in the field of quantum optics. Motivated by one such experiment we investigate a Josephson qubit coupled to a slow LC oscillator with frequency much lower than the qubit's energy splitting. The qubit is ac-driven to perform Rabi oscillations, and the Rabi frequency is tuned to resonance with the oscillator. The properties of this driven circuit QED system depend strongly on relaxation and decoherence effects in the qubit. We investigate both one-photon and two-photon qubit-oscillator coupling, the latter being dominant at the symmetry point of the qubit. When the qubit driving frequency is blue detuned, we find that the system exhibits lasing behavior; for red detuning the qubit cools the oscillator. Similar behavior is expected in an accessible range of parameters for a Josephson qubit coupled to a nano-mechanical oscillator. In a different parameter regime, furthering the analogies between superconducting and quantum optical systems, we investigate Sisyphus damping, which is the key element of the Sisyphus cooling protocol, as well as its exact opposite, Sisyphus amplification.

Keywords: <Driven circuit QED systems, single-qubit lasing, dissipation>
PACS: 85.25.Cp, 42.55.Ah, 85.25.Hv, 85.85.+j

INTRODUCTION

Several experiments on quantum state engineering with superconducting circuits realized concepts originally introduced in the field of quantum optics, as well as extensions thereof, e.g., to the regime of strong coupling [1, 2, 3, 4, 5, 6, 7, 8], and prompted substantial theoretical activities [9, 10, 11, 12, 13, 14, 15, 16, 17, 18, 19]. Josephson qubits play the role of two-level atoms while electric or nanomechanical oscillators play the role of the quantized radiation field. In most QED or circuit QED experiments the atom or qubit transition frequency is near resonance with the oscillator. In contrast, in the experiments of Ref. [1], with setup shown in Fig. 1, the qubit is coupled to a slow LC oscillator with frequency ($\omega_T/2\pi \sim$ MHz) much lower than the qubit's level splitting ($\Delta E/2\pi\hbar \sim 10$ GHz). The idea of this experiment is to drive the qubit at resonance to perform Rabi oscillations with the low Rabi frequency in resonance with the oscillator, $\Omega_R \approx \omega_T$. Indeed, a strong enhancement of the oscillator oscillation amplitude was observed.

In the experiments, in order to minimize decoherence effects, the Josephson flux qubit was biased near the flux degeneracy point. At this symmetry point also the coupling to the oscillator is tuned to zero, and the enhancement should vanish. However, as we will demonstrate in this article, a quadratic coupling to the oscillator near the resonance condition $\Omega_R \approx 2\omega_T$ can explain the observed enhancement [18]. For comparison, and to cover both the regime at and away from the symmetry point, we will consider in the following both linear and quadratic coupling. We find a strong effect, since for blue detuning of the high-frequency driving a population inversion is created in the dressed states of the qubit, and

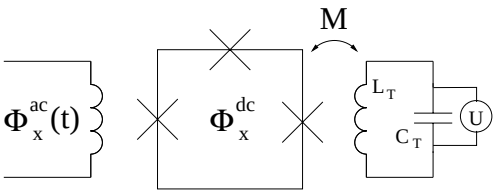

FIGURE 1. In the setup of Ref. [1] an externally driven three-junction flux qubit is coupled inductively to an LC oscillator.

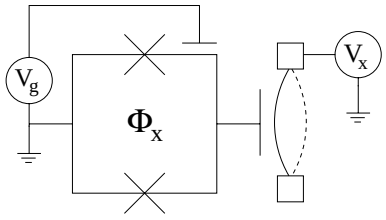

FIGURE 2. A charge qubit is coupled to a nano-mechanical resonator.

the system becomes a "single-atom laser" at the resonance $\Omega_R \approx \omega_T$, or a "single-atom-two-photon laser" for $\Omega_R \approx 2\omega_T$ [20, 21]. In both cases the lasing threshold is reached for realistic system parameters, and the number of quanta in the oscillator is increased considerably. [1] We further note that for red detuning of the qubit's driving the qubit cools the oscillator [18].

In experiments with the same setup as shown in Fig. 1 but in a different parameter regime the mechanisms of Sisyphus cooling and amplification has recently been demonstrated [7]. Due to the resonant high-frequency driving of the qubit, depending on the detuning, the oscillator is either cooled or amplified with a tendency towards lasing. The Sisyphus mechanism is most efficient when the relaxation rate of the qubit is close to the oscillator's frequency. In contrast, the "single-atom laser" and the "single-atom-two-photon laser" situations described above are optimized in the "resolved sub-band" regime where the dissipative transition rates of the qubit are still much lower than the oscillator's frequency.

Also in situations where the resonator is a nanomechanical oscillator (Fig. 2) the driven qubit either cools or amplifies the oscillator. On one hand, this may constitute an important tool on the way to ground state cooling. [2] On the other hand, this setup provides a realization of what is called a SASER [26].

Lasing and cooling of the oscillator have also been observed in a slightly different setup, when the *ac*-driven qubit is replaced by a driven superconducting single-electron transistor biased near the Josephson quasiparticle cycle [27, 28, 29]. When the SSET is coupled to a nanomechanical or electric oscillator it can be used to either cool the oscillator [30, 31, 32, 33, 34, 35] or to produce laser-like behavior. The latter has recently been observed in experiments [36].

The properties of the driven circuit QED system depend strongly on relaxation and decoherence effects in the qubit. This emphasis of the present work is devoted to the study of these dissipative effects.

[1] A related situation, called "dressed-state lasing", had been studied before in quantum optics [22, 23]. The present scenario differs from that one in so far as the resonator modes are coupled to the low-frequency Rabi oscillations rather than to the high-frequency Mollow transitions. The Rabi frequency can be readily tuned to resonance with the oscillator, which should facilitate reaching the lasing threshold and a proper lasing state. A similar idea has been explored in Ref. [24] in connection with coupling of atoms.

[2] A similar strategy for cooling of a nanomechanical resonator via a Cooper pair box qubit has been recently suggested in Ref. [25].

THE SYSTEM HAMILTONIAN

The system to be considered is shown in Fig. 1. A flux qubit is coupled to an electric oscillator and driven to perform Rabi oscillations. The coherent dynamics of the system is described by the Hamiltonian

$$\begin{aligned} H &= -\frac{1}{2}\varepsilon\left(\Phi_x^{dc}\right)\sigma_z - \frac{1}{2}\Delta\sigma_x - \hbar\Omega_{R0}\cos(\omega_d t)\,\sigma_z \\ &\quad + \hbar\omega_T\, a^\dagger a \;+\; g\,\sigma_z\left(a+a^\dagger\right)\;. \end{aligned} \tag{1}$$

The first two terms describe the qubit, with Pauli matrices $\sigma_{x,z}$ operating in the flux basis of the qubit. The energy bias between the flux states $\varepsilon(\Phi_x^{dc})$ is controlled by an external DC magnetic flux, and Δ is the tunneling amplitude between the basis states. The resulting level spacing $\Delta E \equiv \sqrt{\varepsilon^2+\Delta^2}$ typically lies in the range of several GHz. The third term accounts for the driving of the qubit by an applied AC magnetic flux with amplitude Ω_{R0} and frequency ω_d. The last two terms describe the oscillator with frequency $\omega_T = 1/\sqrt{L_T C_T}$, which for the experiments of of Ref. [1] lies in the range of several 10 MHz, as well as the qubit-oscillator interaction. We estimate the coupling constant $g \approx M I_p I_{T,0}$ to be of the order of 10 MHz. Here M is the mutual inductance, I_p the magnitude of the persistent current in the qubit, and $I_{T,0} = \sqrt{\hbar\omega_T/2L_T}$ the amplitude of the vacuum fluctuation of the current in the LC oscillator.

After transformation to the eigenbasis of the qubit, which is the natural basis for the description of the dissipation, the Hamiltonian reads

$$\begin{aligned} H &= -\frac{1}{2}\Delta E\,\sigma_z - \hbar\Omega_{R0}\cos(\omega_d t)\,(\sin\zeta\,\sigma_z - \cos\zeta\,\sigma_x) \\ &\quad + \hbar\omega_T\, a^\dagger a \;+ g\,(\sin\zeta\,\sigma_z - \cos\zeta\,\sigma_x)\left(a+a^\dagger\right)\;, \end{aligned} \tag{2}$$

with $\tan\zeta = \varepsilon/\Delta$ and $\Delta E \equiv \sqrt{\varepsilon^2+\Delta^2}$.

Because of the large difference in energies, $\Delta E \gg \hbar\omega_T$, it is tempting, in the spirit of the usual rotating wave approximation (RWA), to drop the transverse coupling term $-g\cos\zeta\,\sigma_x\left(a+a^\dagger\right)$ of Eq. (2). However, near the symmetry point (where $\sin\zeta = 0$) the longitudinal coupling is weak. Therefore, we retain the former but transform it by employing a Schrieffer-Wolff transformation, $U_S = \exp(iS)$, with generator $S = (g/\Delta E)\cos\zeta\,\left(a+a^\dagger\right)\sigma_y$, into a second-order longitudinal coupling. On the other hand, since $\hbar\omega_d \sim \Delta E$, we can drop within RWA the longitudinal driving term $-\hbar\Omega_{R0}\cos(\omega_d t)\sin\zeta\,\sigma_z$. The Hamiltonian then reads

$$\begin{aligned} H &= -\frac{1}{2}\Delta E\,\sigma_z + \hbar\Omega_{R0}\cos(\omega_d t)\cos\zeta\,\sigma_x + \hbar\omega_T\, a^\dagger a \\ &\quad + g\sin\zeta\,\sigma_z\left(a+a^\dagger\right) - \frac{g^2}{\Delta E}\cos^2\zeta\,\sigma_z\left(a+a^\dagger\right)^2 . \end{aligned} \tag{3}$$

A further unitary transformation with $U_R = \exp(-i\omega_d\sigma_z t/2)$ brings the Hamiltonian to the rotating

frame, $\tilde{H} \equiv U_R H U_R^\dagger + i\hbar \dot{U}_R U_R^\dagger$. After diagonalization of the qubit terms we obtain

$$\begin{aligned}\tilde{H} &= -\frac{1}{2}\hbar\Omega_R\,\sigma_z + \hbar\omega_T\, a^\dagger a \\ &+ g\sin\zeta\,\left[\sin\beta\,\sigma_z - \cos\beta\,\sigma_x\right]\left(a + a^\dagger\right) \\ &- \frac{g^2}{\Delta E}\cos^2\zeta\,\left[\sin\beta\,\sigma_z - \cos\beta\,\sigma_x\right]\left(a + a^\dagger\right)^2 . \quad (4)\end{aligned}$$

Here $\Omega_R = \sqrt{\Omega_{R0}^2\cos^2\zeta + \delta\omega^2}$, where $\delta\omega \equiv \omega_d - \Delta E/\hbar$ is the detuning, and $\tan\beta = \delta\omega/(\Omega_{R0}\cos\zeta)$.

Finally we employ a second RWA. While the first one dropped terms oscillating with frequencies of order $\Delta E/\hbar$, the second one assumes the Rabi frequency Ω_R and the oscillator frequency ω_T to be fast. In the interaction representation with respect to the non-interacting Hamiltonian, $\tilde{H}_0 = (\hbar\Omega_R/2)\sigma_z + \hbar\omega_T\, a^\dagger a$, we then obtain

$$\begin{aligned}\tilde{H}_I &= g_1\left(a^\dagger\sigma_- e^{-i(\Omega_R-\omega_T)t} + h.c.\right) \\ &+ g_2\left(a^{\dagger 2}\sigma_- e^{-i(\Omega_R-2\omega_T)t} + h.c.\right) \\ &+ g_3\left(a^\dagger a + a a^\dagger\right)\sigma_z . \quad (5)\end{aligned}$$

We kept both single-photon and two-photon interactions with $g_1 = -g\sin\zeta\cos\beta$ and $g_2 = (g^2/\Delta E)\cos^2\zeta\cos\beta$, although within RWA only one of them survives: the single-photon term for $\Omega_R \sim \omega_T$, or the two-photon term for $\Omega_R \sim 2\omega_T$. The last term of (5) with $g_3 = -(g^2/\Delta E)\cos^2\zeta\sin\beta$ is the *ac*-Stark effect, causing a qubit state dependent frequency shift of the oscillator [37]. In what follows we will assume that the qubit is kept near the symmetry point, i.e., $\varepsilon \ll \Delta$ and $\cos\zeta \simeq 1$.

DISSIPATION IN THE DRIVEN SYSTEM

The transformation to "dressed states" in the rotating frame modifies the relaxation, excitation and decoherence rates as compared to the standard results. To illustrate these effects and justify the treatment of the dissipation in latter sections we first consider a driven qubit (ignoring the coupling to the oscillator) coupled to a bath observable $\hat{X}$,

$$\begin{aligned}H &= -\frac{1}{2}\Delta E\,\sigma_z + \hbar\Omega_{R0}\cos(\omega_d t)\,\sigma_x \\ &- \frac{1}{2}\left(b_x\sigma_x + b_y\sigma_y + b_z\sigma_z\right)\hat{X} + H_{\rm bath} . \quad (6)\end{aligned}$$

In the absence of driving, $\Omega_{R0} = 0$, and for regular power spectra of the fluctuating bath observables we can proceed using Golden rule arguments. The transverse noise is responsible for the relaxation and excitation with rates

$$\begin{aligned}\Gamma_\downarrow &= \frac{|b_\perp|^2}{4\hbar^2}\langle\hat{X}^2\rangle_{\omega=\Delta E} \\ \Gamma_\uparrow &= \frac{|b_\perp|^2}{4\hbar^2}\langle\hat{X}^2\rangle_{\omega=-\Delta E} , \quad (7)\end{aligned}$$

while longitudinal noise produces a pure dephasing with rate [38]

$$\Gamma_\varphi^* = \frac{|b_z|^2}{2\hbar^2}S_X(\omega=0) . \quad (8)$$

Here $b_\perp \equiv b_x + ib_y$, and we introduced the ordered correlation function $\langle\hat{X}^2\rangle_\omega \equiv \int dt\; e^{i\omega t}\langle\hat{X}(t)\hat{X}(0)\rangle$, as well as the power spectrum, i.e., the symmetrized correlation function, $S_X(\omega) \equiv (\langle\hat{X}^2\rangle_\omega + \langle\hat{X}^2\rangle_{-\omega})/2$. The rates (7) and (8) also define the relaxation rate $1/T_1 = \Gamma_1 = \Gamma_\downarrow + \Gamma_\uparrow$ and the total dephasing rate $1/T_2 = \Gamma_\varphi = \Gamma_1/2 + \Gamma_\varphi^*$ which appear in the Bloch equations.

To account for the driving with frequency ω_d it is convenient to transform to the rotating frame via a unitary transformation $U_R = \exp(-i\omega_d\sigma_z t/2)$. Within RWA the transformed Hamiltonian reduces to

$$\begin{aligned}\tilde{H} &= \frac{1}{2}\hbar\left[\Omega_{R0}\sigma_x + \delta\omega\sigma_z\right] \quad (9)\\ &- \frac{1}{2}\left[b_z\sigma_z + b_\perp e^{i\omega_d t}\sigma_- + b_\perp^* e^{-i\omega_d t}\sigma_+\right]\hat{X} + H_{\rm bath} ,\end{aligned}$$

where $b_\perp \equiv b_x + ib_y$, and the detuning is $\delta\omega \equiv \omega_d - \Delta E/\hbar$. Diagonalizing the first line of (9) one obtains

$$\begin{aligned}&\tilde{H} = \frac{1}{2}\hbar\Omega_R\,\sigma_z + H_{\rm bath} \\ &-\left[\frac{\sin\beta}{2}\,b_z + \frac{\cos\beta}{4}\left(b_\perp^* e^{-i\omega_d t} + b_\perp e^{i\omega_d t}\right)\right]\sigma_z\hat{X} \\ &-\Big\{\Big[\frac{(\sin\beta+1)}{4}\,b_\perp^* e^{-i\omega_d t} + \frac{(\sin\beta-1)}{4}\,b_\perp e^{i\omega_d t} \\ &-\frac{\cos\beta}{2}\,b_z\Big]\sigma_+\hat{X} + h.c.\Big\} , \quad (10)\end{aligned}$$

with $\Omega_R = \sqrt{\Omega_{R0}^2 + \delta\omega^2}$ and $\tan\beta = \delta\omega/\Omega_{R0}$. From here Golden-rule arguments yield the relaxation and excitation rates in the rotating frame [38]. For a sufficiently regular power spectrum of fluctuations at frequencies of order $\omega \approx \pm\Delta E/\hbar$ we can ignore the effect of detuning and the small shifts by $\pm\Omega_R$ as compared to the high frequency $\omega_d \approx \Delta E/\hbar$. We further assume that $\Omega_R \ll k_B T/\hbar$. In this case we find the simple relations

$$\begin{aligned}\tilde{\Gamma}_\uparrow &= \frac{(1+\sin\beta)^2}{4}\Gamma_\downarrow + \frac{(1-\sin\beta)^2}{4}\Gamma_\uparrow + \frac{1}{2}\cos^2\beta\,\Gamma_v , \\ \tilde{\Gamma}_\downarrow &= \frac{(1-\sin\beta)^2}{4}\Gamma_\downarrow + \frac{(1+\sin\beta)^2}{4}\Gamma_\uparrow + \frac{1}{2}\cos^2\beta\,\Gamma_v , \\ \tilde{\Gamma}_\varphi^* &= \sin^2\beta\,\Gamma_\varphi^* + \frac{\cos^2\beta}{2}(\Gamma_\downarrow + \Gamma_\uparrow) , \quad (11)\end{aligned}$$

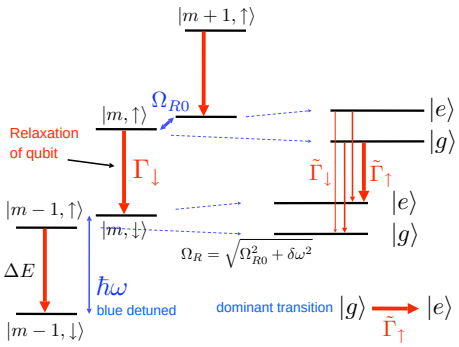

FIGURE 3. Dressed states of a driven qubit near resonance. Here m is the number of photons of the driving field, which is assumed to be quantized.

where the rates in the lab frame are given by Eq. (7) and a new rate appears, $\Gamma_\nu \equiv \frac{1}{2} b_z^2 S_X(\Omega_R)$, which depends on the power spectrum at the Rabi frequency.

The ratio of up- and down-transitions depends on the detuning and can be expressed by an effective temperature. Right on resonance, where $\beta = 0$, we have $\tilde{\Gamma}_\uparrow = \tilde{\Gamma}_\downarrow$, corresponding to infinite temperature or a classical drive. For "blue" detuning, $\beta > 0$, we find $\tilde{\Gamma}_\uparrow > \tilde{\Gamma}_\downarrow$, i.e., *negative temperature*. This leads to a population inversion of the qubit, which is the basis for the lasing behavior which will be described below.

To illustrate how the population inversion is created for blue detuning we show in Fig. 3 the level structure, i.e., the formation of dressed states, of a near-resonantly driven qubit. For the purpose of this explanation the driving field is quantized. This level structure was described first by Mollow [23]. The picture also illustrates how for blue detuning a pure relaxation process, $\Gamma_\downarrow = \Gamma_0$, in the laboratory frame predominantly leads to an excitation process, $\tilde{\Gamma}_\uparrow$, in the rotating frame.

Within the approximation described in the previous section the Liouville equation governing the dynamics of the density matrix in the rotating frame can be presented in a simple Lindblad form. In the lab frame the dissipation is accounted for by two damping terms,

$$\dot{\rho} = -\frac{i}{\hbar}[H,\rho] + L_Q\rho + L_R\rho \ , \qquad (12)$$

where the qubit's dissipation is described by

$$\begin{aligned} L_Q\rho &= \frac{\Gamma_\downarrow}{2}(2\sigma_-\rho\sigma_+ - \rho\sigma_+\sigma_- - \sigma_+\sigma_-\rho) \\ &+ \frac{\Gamma_\uparrow}{2}(2\sigma_+\rho\sigma_- - \rho\sigma_-\sigma_+ - \sigma_-\sigma_+\rho) \\ &+ \frac{\Gamma_\varphi^*}{2}(\sigma_z\rho\sigma_z - \rho) \ , \end{aligned} \qquad (13)$$

with rates given by (7) and (8). The resonator damping, with strength parametrized by κ, can be written as [39]

$$\begin{aligned} L_R\rho = \ & \frac{\kappa}{2}(N_{\rm th}+1)\left(2a\rho a^\dagger - a^\dagger a\rho - \rho a^\dagger a\right) \\ & + \frac{\kappa}{2}N_{\rm th}\left(2a^\dagger\rho a - aa^\dagger\rho - \rho aa^\dagger\right) \ . \end{aligned} \qquad (14)$$

Here $N_{\rm th} = 1/\left[\exp(\hbar\omega_T/k_BT) - 1\right]$ is the thermal distribution function of photons in the resonator.

After transformation to the rotating frame and RWA the Liouville equation again has a Lindblad form. In the interaction representation it is

$$\dot{\tilde{\rho}} = -\frac{i}{\hbar}\left[\tilde{H}_I, \tilde{\rho}\right] + \tilde{L}_Q\tilde{\rho} + L_R\tilde{\rho} \ , \qquad (15)$$

The qubit damping term $\tilde{L}_Q\tilde{\rho}$ has the same form as (13) except that the rates are those in the rotating frame (11), while the oscillator damping term is not affected by the transformation. Although at low temperatures in the lab frame the relaxation processes dominate, the transformation to the rotating frame introduces excitation and pure dephasing processes.

THE SINGLE-QUBIT LASER

In the following we will consider two resonance situations, $\Omega_R \sim \omega_T$ or $\Omega_R \sim 2\omega_T$, when either the one- or the two-photon interactions dominate, and investigate the effects of blue or red detuning, $\delta\omega \equiv \omega_d - \Delta E/\hbar$, of the qubit driving frequency. We also study the effects of detuning of the Rabi frequency Ω_R relative to that of the oscillator.

One-photon interaction

When the Rabi frequency is in resonance with the oscillator, $\Omega_R \approx \omega_T$, the Hamiltonian (5) in RWA reduces to

$$\begin{aligned} H_I &= g_1\left(a^\dagger\sigma_- e^{-i(\Omega_R-\omega_T)t} + h.c.\right) \\ &+ g_3\left(a^\dagger a + aa^\dagger\right)\sigma_z \ . \end{aligned} \qquad (16)$$

From here we proceed in the frame of the standard semiclassical approach of laser physics [40, 39] with the following main steps: In the absence of fluctuations the system is described by Maxwell-Bloch equations for the classical variables $\alpha = \langle a\rangle$, $\alpha^* = \langle a^\dagger\rangle$, $\langle\sigma_\pm\rangle$ and $\langle\sigma_z\rangle$, which can be derived from the Hamiltonian (16) if all correlation functions are assumed to factorize. Next the qubit variables can be adiabatically eliminated as long as $\kappa, g_1 \ll \tilde{\Gamma}_1, \tilde{\Gamma}_\varphi$, which leads to a closed equation of motion for α. If we finally account for fluctuations, e.g., due

to thermal noise in the resonator, α becomes a stochastic variable obeying a Langevin equation [39],

$$\dot{\alpha} = \left[\frac{C}{\tilde{\Gamma}_\varphi + i\delta\Omega} s_z^{st} - \kappa - 4ig_3 s_z^{st} \right] \frac{\alpha}{2} + \xi(t) . \qquad (17)$$

Here $C \equiv 2g_1^2$, $s_z^{st} = -D_0/\left(1+|\alpha^2|/\tilde{n}_0\right)$ is the stationary value of the population difference between the qubit levels, and $D_0 = \left(\tilde{\Gamma}_\downarrow - \tilde{\Gamma}_\uparrow\right)/\tilde{\Gamma}_1$ is the normalized difference between the rates with $\tilde{\Gamma}_1 = \tilde{\Gamma}_\uparrow + \tilde{\Gamma}_\downarrow$. We further introduced the photon saturation number $n_0 = \tilde{\Gamma}_\varphi \tilde{\Gamma}_1/4g_1^2$ and $\tilde{n}_0 \equiv n_0(1+\delta\Omega^2/\tilde{\Gamma}_\varphi^2)$, and the total dephasing rate $\tilde{\Gamma}_\varphi = \tilde{\Gamma}_1/2 + \tilde{\Gamma}_\varphi^*$. The detuning of the Rabi frequency enters in combination with a frequency renormalization, $\delta\Omega \equiv \Omega_R - \omega_T + g_3|\alpha|^2$. The Langevin force due to thermal noise in the oscillator satisfies $\langle \xi(t)\xi^*(t')\rangle = \kappa N_{\rm th}\delta(t-t')$ and $\langle \xi(t)\xi(t')\rangle = 0$. Noise originating from the qubit can be neglected provided the thermal noise is strong, $\kappa N_{\rm th} \gg g_1^2/\tilde{\Gamma}_\varphi$.

Two-photon interaction

The two-photon effect dominates near the resonance $\Omega_R \approx 2\omega_T$. In RWA the Hamiltonian reduces to

$$\begin{aligned} H_I &= g_2\left(a^{\dagger 2}\sigma_- e^{-i(\Omega_R - 2\omega_T)t} + h.c.\right) \\ &+ g_3\left(a^\dagger a + a a^\dagger\right)\sigma_z . \end{aligned} \qquad (18)$$

The corresponding Langevin equation for the resonator reads

$$\dot{\alpha} = \left[\frac{C}{\tilde{\Gamma}_\varphi + i\delta\Omega} s_z^{st} - \kappa - 4ig_3 s_z^{st} \right] \frac{\alpha}{2} + \xi(t) , \qquad (19)$$

i.e., is of the same form as Eq. (17) but with $C \equiv 4g_2^2|\alpha|^2$ and $s_z^{st} = -D_0/\left(1+(|\alpha^2|/\tilde{n}_0)^2\right)$. The photon saturation number is now given by $n_0 = (\tilde{\Gamma}_\varphi\tilde{\Gamma}_1/4g_2^2)^{1/2}$, and $\tilde{n}_0 \equiv n_0(1+\delta\Omega^2/\tilde{\Gamma}_\varphi^2)^{1/2}$. Again $\xi(t)$ represents thermal noise, while noise arising from the qubit can be neglected if $\kappa N_{\rm th} \gg g_2^2\bar{n}/\tilde{\Gamma}_\varphi$. The detuning of the Rabi frequency for two-photon interaction is given by $\delta\Omega \equiv \Omega_R - 2\omega_T + g_3|\alpha|^2$.

Results from the Langevin equation

Eqs. (17) and (19), written as $\dot{\alpha} = -f(n)\alpha/2 + \xi(t)$, can be transformed to equations for the average number of photons $\langle|\alpha|^2\rangle = \bar{n}$ in the form $\dot{\bar{n}} = -\langle n{\rm Re}[f(n)]\rangle + \kappa N_{\rm th}$. In the steady state, for $\bar{n} \gg 1$ they can be approximated by $\bar{n}{\rm Re}[f(\bar{n})] = \kappa N_{\rm th}$. The results of this analysis are shown in Fig. 4. To demonstrate both the one-photon and two-photon effects we assume a small deviation from the symmetry point, $\varepsilon = 0.01\Delta$. The two-photon resonance (the outer one) persist for $\varepsilon = 0$, while the one-photon resonance (the inner one) vanishes there. We observe that the solutions show bistability bifurcations (see below). The sharp drops of $\bar{n}$ seen in Fig. 4 emerge as only the lowest stable value is plotted .

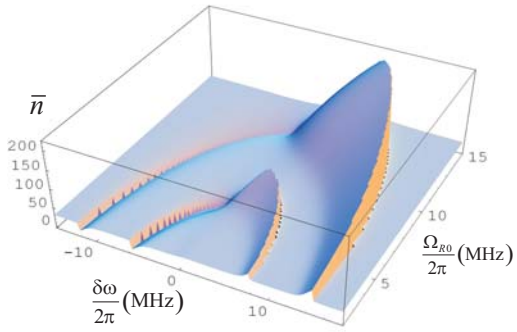

FIGURE 4. Average number of photons in the resonator as function of the driving detuning $\delta\omega$ and amplitude Ω_{R0}. Peaks at $\delta\omega > 0$ correspond to lasing, while dips at $\delta\omega < 0$ correspond to cooling. The inner curve corresponds to the one-photon resonance which exists only away from the symmetry point. Here we assumed $\varepsilon = 0.01\Delta$. The outer curve describes the two-photon resonance, which persists at $\varepsilon = 0$. In domains of bistability the lowest value of $\bar{n}$ is plotted (leading to the sharp drops in both curves). We chose the following parameters for the qubit: $\Delta/2\pi = 1$ GHz, $\varepsilon = 0.01\Delta$, $\Gamma_0/2\pi = 125$ kHz, the resonator: $\omega_T/2\pi = 6$MHz, $\kappa/2\pi = 0.34$ kHz, and the coupling: $g/2\pi = 3.3$ MHz. The bath temperature is $T = 10$ mK.

Solution of the master equation

We also solved the full master equation (15) numerically, which provides access not only to the average number of photons in the oscillator, $\bar{n}$, but also to the whole distribution function $P(n)$. To reach convergence with a limited number of photon basis states ($n \leq 100$) we assumed a low thermal number, $N_{\rm th} = 5$ and a relatively high relaxation constant of the oscillator $\kappa/2\pi =$ 1.7 kHz. In Fig. 5 the solutions of the Langevin equations (17) and (19) and those of the master equation (15) is compared.

In Fig. 6 the distribution function, $P(n)$, for the number of photons in the oscillator is plotted both for the cooling and enhancement regime. For comparison also the thermal (Bose-Einstein) distribution is plotted.

The enhancement and cooling effects described here rely crucially on the transition rates, i.e., the dissipative effects as described by the Liouville equations. In order to demonstrate this dependence we show in Fig. 7 the dependence of the average photon number on the

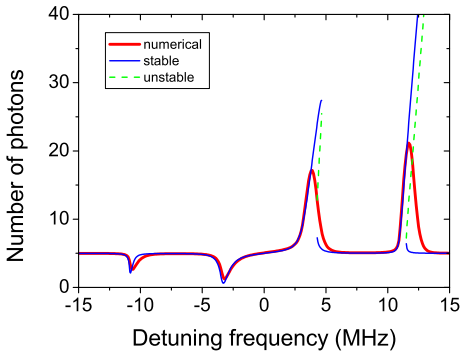

FIGURE 5. Average number of photons $\bar{n}$ versus the detuning. The blue curves are obtained from the Langevin equations (17) and (19). They show the bistability with the solid curve denoting stable solutions, while the dashed curve denotes the unstable one. The red curve is obtained from the master equation (15). The driving amplitude is taken as $\Omega_{R0}/2\pi = 5$MHz. The parameters are for the qubit: $\Delta/2\pi = 1$ GHz, $\varepsilon = 0.01\Delta$, $\Gamma_0/2\pi = 125$ kHz, the resonator: $\omega_T/2\pi = 6$MHz, $\kappa/2\pi = 1.7$ kHz, $N_{\rm th} = 5$, and the coupling: $g/2\pi = 3.3$ MHz.

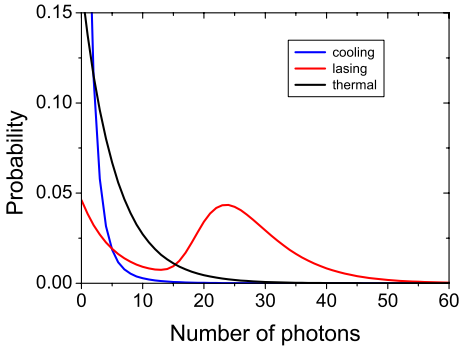

FIGURE 6. The distribution function, $P(n)$, obtained form the master equation (15). Blue curve: cooling regime of the one-photon resonance with $\Omega_{R0} = 2\pi \times 5$MHz and $\delta\omega = -2\pi \times 3.2$MHz. Red curve: lasing regime of the two-photon resonance with $\Omega_{R0} = 2\pi \times 5$MHz and $\delta\omega = 2\pi \times 11.7$MHz. The peak in the $P(n)$ distribution between $n = 20$ and 30 is related to the lasing behavior. Black curve: thermal distribution with $N_{\rm th} = 5$. The parameters are as in Fig. 5.

qubit's relaxation rate at the one-photon resonance. We note a non-monotonic dependence on the qubit's relaxation rate. Above the saturation threshold for $\bar{n} > n_0$ the pumping rate is limited by Γ_0, leading to a roughly linear growth of the photon number with increasing Γ_0. At the saturation threshold for $\bar{n} \sim n_0$ the effective coupling is determined by g_1 and the photon number becomes insensitive to small variations of Γ_0. Finally, for $\bar{n} < n_0$, an increase of Γ_0 predominantly increases the dephasing rate $\tilde{\Gamma}_\varphi$. As can be seen from Eq. (17) this destroys the coherent coupling between qubit and oscillator and the photon number decreases towards N_{th}. In Figure 7 we plot both the results of a numerical solution of the master equation and the Langevin approximation. We find good agreement between both in the considered parameter range.

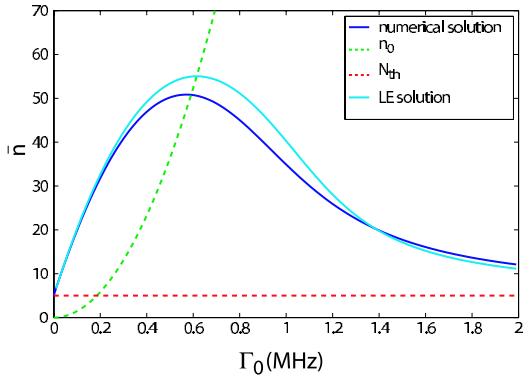

FIGURE 7. Average number of photons in the resonator as function of the qubit's relaxation rate, Γ_0 at the one-photon resonance, $\Omega_R = \omega_T$ for $g_3 = 0$ and $N_{th} = 5$. The dark blue line shows the numerical solution of the master equation, the light blue solid line represents the solution of the Langevin equation, Eq. (17). The green and red dashed curves represent respectively the saturation number n_0 and the thermal photon number $N_{\rm th}$. The parameters are as in Fig. 5 (except for Γ_0).

SISYPHUS COOLING AND AMPLIFICATION

In experiments with the same setup as shown in Fig. 1a) – but in a different parameter regime when the relaxation rate of the qubit is close to the oscillator's driving frequency – the mechanisms of *Sisyphus* cooling and amplification [41] has recently been demonstrated [7]. In these experiments the *LC* tank circuit is driven near-resonantly by a low-frequency *ac* current, and its response, which is influenced by the high-frequency driven qubit, is detected. For red-detuned high-frequency driving of the qubit the low-frequency *LC*-circuit carries out work in its forward and backward oscillation cycle, always increasing the energy of the qubit (similar to Sisyphus always pushing up a rock). This produces additional damping and a reduction of the effective quality factor, which can be associated with cooling of the oscillator. For blue-detuned qubit driving, the same mechanism leads to Sisyphus amplification ("lucky Sisyphus" rolling down the rock) and a precursor of lasing of the resonator. It is accompanied by an enhancement of the effective quality factor. These effects were confirmed in the second series of experiments where the power spectrum of the oscilla-

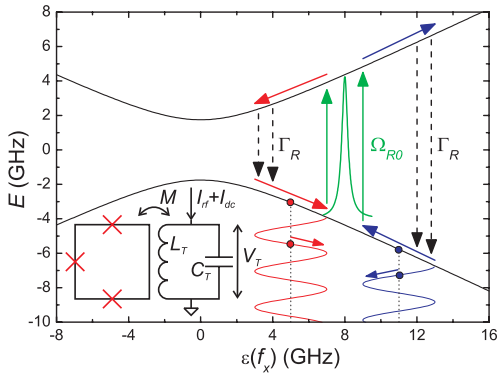

FIGURE 8. The energy levels of the qubit as a function of the energy bias of the qubit $\varepsilon(f_x) = 2\Phi_0 I_p f_x$. The sinusoidal current in the tank coil, indicated by the wavy line, drives the bias of the qubit. The starting point of the cooling (heating) cycles is denoted by blue (red) dots. The resonant excitation of the qubit due to the high-frequency driving, characterized by Ω_{R0}, is indicated by two green arrows and by the Lorentzian depicting the width of this resonance. The relaxation of the qubit is denoted by the black dashed arrows. The inset shows a schematic of the qubit coupled to an LC circuit. The high frequency driving is provided by an on-chip microwave antenna. (Figure taken from Ref. [7].)

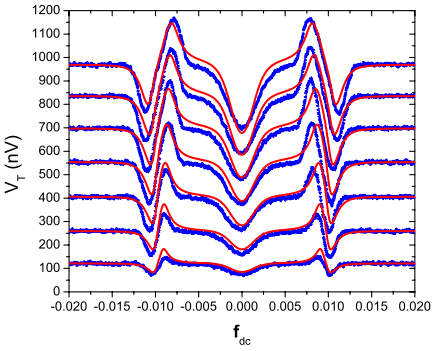

FIGURE 9. Blue lines: experimental data, red lines: numerical solution of Eqs. (15) for $\Omega_{R0} = 2\pi \times 0.5$ GHz, $\Gamma_R = 1.0 \cdot 10^8 s^{-1}$, $\Gamma_\varphi^* = 5.0 \cdot 10^9 s^{-1}$ and different strength of the resonator driving, as indicated by the asymptotic values. The central dip is due to the quadratic coupling term in (3) which causes a shift of the oscillator frequency.(Figure taken from Ref. [7].)

tor, i.e., the number of photons and the line-width, were measured directly.

The operation principle is illustrated in Fig. 8. The eigenenergies of the flux qubit eigenstates are plotted versus the flux bias Φ_x. The system is operated in the vicinity of the degeneracy point, $f_x \equiv \Phi_x/\Phi_0 - 1/2 \approx 0$. The coupling of the oscillator to the qubit, incl. its low-frequency driving in an adiabatic approximation, can be included via a contribution to the external flux Φ_x. I.e., the current in the tank circuit shifts the bias flux of the qubit by $\Phi_x(t) = M[I_{dc} + I_{\rm rf}(t)]$. We first describe the damping (cooling, hence marked in blue) for a situation where the driving is red-detuned, $\hbar\omega_d < \Delta E$; the amplification (marked in red) for blue-detuning can be described in an analogous way. The oscillations of the current in the tank circuit, $I_{\rm rf}(t)$, lead to oscillations of $\varepsilon(f_x)$ around a value determined by the dc component, I_{dc}. In the first part of the cycle, when the qubit is in the ground state, the current shifts the qubit towards the resonance, $\Delta E = \hbar\omega_d$, i.e., the energy of the qubit grows due to work done by the LC circuit. Once the system reaches the vicinity of the resonance point, the qubit can get excited, the energy being provided by the high-frequency driving field. With parameters adjusted such that this happens at the turning point of the oscillating trajectory, the qubit in the excited state is now shifted by the current away from the resonance, such that the qubit's energy continues to grow. Again the work has to be provided by the LC circuit. The cycle is completed by a relaxation process which takes the qubit back to the ground state. The maximum effect is achieved when the driving frequency and relaxation rate are of the same order of magnitude. Note that the complete cycle resembles the ideal Otto-engine thermodynamic cycle [42].

We solve the master equation (15) numerically in the quasi-classical limit, i.e., for $n \equiv \langle a^\dagger a \rangle \gg 1$, and for various choices of the parameters Γ_R, Γ_φ^*, and Ω_{R0}. As the system is harmonically driven, we determine the response of the observables/density matrix at the driving frequency, and, finally, find the amplitude of the driven voltage oscillations across the tank circuit. As shown in Fig. 9 by fitting the system parameters within a reasonable range we reproduce well the experimental findings.

RESULTS AND DISCUSSION

We summarize our main conclusions. Our results for the number of photons $\bar{n}$ are plotted in Fig. 4 as a function of the detuning $\delta\omega$ of the driving frequency and driving amplitude Ω_{R0}. It exhibits sharp structures along two curves corresponding to the one- and two-photon resonance conditions, $\Omega_R = \omega_T - g_3\bar{n}$ and $\Omega_R = 2\omega_T - g_3\bar{n}$. Blue detuning, $\delta\omega > 0$, induces a strong population inversion of the qubit levels, which in resonance leads to one-qubit lasing. In experiments the effect can be measured as a strong increase of the number of photons in the resonator above the thermal values. Red detuning produces a one-qubit cooler with resulting photon numbers substantially below the thermal value.

The bistability of the solution of the Langevin description is illustrated in Fig. 5. In the range of bistability we expect a telegraph-like noise corresponding to the random switches between the two solutions.

Potentially useful applications of the considered scheme are the lasing behavior and the creation of a highly non-thermal population of the oscillator as well as the cooling. Within the accuracy of our approach we estimate that a population of order $\bar{n} = 1$ can be reached for optimal detuning. A more detailed analysis is required to determine the precise cooling limit.

In Ref. [7] a reduction of order 10% in the number of photons in the LC circuit was observed due to Sisyphus cooling. The conclusion is that the system is optimized towards maximum Sisyphus damping rather than minimum temperature. Indeed, damping is optimized when the resonant point is reached at the turning point of the oscillators trajectory. In this regime even a small reduction of the oscillators amplitude switches the whole mechanism off. One needs, thus, a feedback mechanism in which the detuning is slightly reduced when the 10% cooling is reached. This would bring the system again into the optimal damping regime with additional cooling.

So far we considered an LC oscillator coupled to a flux qubit, but our analysis equally applies for a nanomechanical resonator coupled capacitively to a Josephson charge qubit (see Fig. 1b). In this case σ_z stands for the charge of the qubit and both the coupling to the oscillator as well as the driving are capacitive, proportional to σ_z. To produce the capacitive qubit-oscillator coupling, the latter could be metal-coated and biased by the voltage source V_x. The dc component of the gate voltage V_g puts the system near the charge degeneracy point where dephasing due to $1/f$ charge noise is minimal. Rabi driving is induced by an *ac* component of V_g. Realistic experimental parameters are expected to be similar to the ones used in the examples discussed above, except that a higher quality factor of the resonator ($\sim 10^5$) and higher number of quanta in the oscillator can be reached. This number will easily exceed the thermal one, thus a proper lasing state with Poisson statistics, appropriately named SASER [26], is produced. One should then observe the usual line narrowing with width given by $\kappa N_{\rm th}/(4\bar{n}) \sim \kappa^2 N_{\rm th}/\tilde{\Gamma}_1$. The experimental observation of this line-width narrowing would constitute a confirmation of the lasing/sasing.

ACKNOWLEDGMENTS

We thank E. Il'ichev, O. Astafiev, A. Blais, M. Devoret, D. Esteve, J. Hauss, C. Hutter, R. Kothari, M. D. LaHaye, Y. Nakamura, F. Nori, E. Solano, K. C. Schwab, F. K. Wilhelm, and S. Yeshwant for fruitful discussions. The work is part of the EU IST Project EuroSQIP.

REFERENCES

1. E. Il'ichev *et al.*, *Phys. Rev. Lett.* **91**, 097906 (2003).
2. A. Wallraff *et al.*, *Nature* **431**, 162 (2004).
3. I. Chiorescu *et al.*, *Nature* **431**, 159 (2004).
4. A. Wallraff *et al.*, *Phys. Rev. Lett.* **95**, 060501 (2005).
5. J. Johansson *et al.*, *Phys. Rev. Lett.* **96**, 127006 (2006).
6. A. Naik *et al.*, *Nature* **443**, 193 (2006).
7. M. Grajcar *et al.*, *Nature Physics* **4**, 612 (2008).
8. F. Deppe *et al.*, *arXiv.org:0805.3294* (2008).
9. O. Buisson *et al.*, *Phys. Rev. Lett.* **90**, 238304 (2003).
10. A. Blais *et al.*, *Phys. Rev. A* **69**, 062320 (2004).
11. Y. Liu, L. F. Wei, and F. Nori, *Europhys. Lett.* **67**, 941 (2004).
12. I. Martin *et al.*, *Phys. Rev. B* **69**, 125339 (2004).
13. K. Moon, and S. M. Girvin, *Phys. Rev. Lett.* **95**, 140504 (2005).
14. M. Mariantoni *et al.*, *cond-mat/0509737* (2005).
15. Y. Liu, C. P. Sun, and F. Nori, *Phys. Rev. A* **74**, 052321 (2006).
16. M. Wallquist, V. S. Shumeiko, and G. Wendin, *Phys. Rev. B* **74**, 224506 (2006).
17. F. Xue *et al.*, *New J. Phys.* **9**, 35 (2007).
18. J. Hauss *et al.*, *Phys. Rev. Lett.* **100**, 037003 (2008).
19. S. Ashhab *et al.*, *arXiv.org:0803.1209* (2008).
20. Y. Mu, and C. M. Savage, *Phys. Rev. A* **46**, 5944–5954 (1992).
21. J. McKeever *et al.*, *Nature* **425**, 268 (2003).
22. J. Zakrzewski, M. Lewenstein, and T. W. Mossberg, *Phys. Rev. A* **44**, 7717 (1991).
23. B. R. Mollow, *Phys. Rev.* **188**, 1969–1975 (1969).
24. D. Jonathan, and M. B. Plenio, *Phys. Rev. Lett.* **87**, 127901 (2001).
25. K. Jaehne, K. Hammerer, and M. Wallquist, *arXiv.org:0804.0603* (2008).
26. A. J. Kent *et al.*, *Phys. Rev. Lett.* **96**, 215504 (2006).
27. T. A. Fulton *et al.*, *Phys. Rev. Lett.* **63**, 1307 (1989).
28. A. Maassen van den Brink, G. Schön, and L. J. Geerligs, *Phys. Rev. Lett.* **67**, 3030 (1991).
29. A. Maassen van den Brink *et al.*, *Z. Physik B* **85**, 459 (1991).
30. Ya. M. Blanter, O. Usmani, and Yu. V. Nazarov, *Phys. Rev. Lett.* **93**, 136802 (2004).
31. M. P. Blencowe, J. Imbers, and A. D. Armour, *New J. Phys.* **7**, 236 (2005).
32. A. A. Clerk, and S. Bennett, *New J. Phys.* **7**, 238 (2005).
33. S. D. Bennett, and A. A. Clerk, *Phys. Rev. B* **74**, 201301 (2006).
34. O. Usmani, Y. M. Blanter, and Y. V. Nazarov, *Phys. Rev. B* **75**, 195312 (2007).
35. D. A. Rodrigues, J. Imbers, and A. D. Armour, *Phys. Rev. Lett.* **98**, 067204 (2007).
36. O. Astafiev *et al.*, *Nature* **449**, 588–590 (2007).
37. Y. S. Greenberg *et al.*, *Phys. Rev. B* **66**, 214525 (2002).
38. G. Ithier *et al.*, *Phys. Rev. B* **72**, 134519 (2005).
39. C. W. Gardiner, and P. Zoller, *Quantum noise*, Springer, 2004, 3-d edn.
40. M. Reid, K. J. McNeil, and D. F. Walls, *Phys. Rev. A* **24**, 2029 (1981).
41. D. J. Wineland, J. Dalibard, and C. Cohen-Tannouji, *J. Opt. Soc.* **B9**, 32 (1992).
42. H. T. Quan *et al.*, *Phys. Rev. E* **76**, 031105 (2007).